View metadata, citation and similar papers at core.ac.uk

brought to you by CORE

provided by Repositorio da Producao Cientifica e Intelectual da Unicamp

UNIVERSIDADE ESTADUAL DE CAMPINAS
SISTEMA DE BIBLIOTECAS DA UNICAMP
REPOSITÓRIO DA PRODUÇÃO CIENTIFICA E INTELECTUAL DA UNICAMP

Versão do arquivo anexado / Version of attached file:

Versão do Editor / Published Version

Mais informações no site da editora / Further information on publisher's website:

https://aip.scitation.org/doi/10.1063/1.4892417

DOI: 10.1063/1.4892417

Direitos autorais / Publisher's copyright statement:

©2014 by AIP Publishing. All rights reserved.

DIRETORIA DE TRATAMENTO DA INFORMAÇÃO

Cidade Universitária Zeferino Vaz Barão Geraldo
CEP 13083-970 – Campinas SP
Fone: (19) 3521-6493
http://www.repositorio.unicamp.br

CrossMark click for updates

Eliminating anchor loss in optomechanical resonators using elastic wave interference

Mian Zhang,[1] Gustavo Luiz,[2] Shreyas Shah,[1] Gustavo Wiederhecker,[2] and Michal Lipson[1,3,a)]
[1]School of Electrical and Computer Engineering, Cornell University, Ithaca, New York 14853, USA
[2]Instituto de Física, Universidade Estadual de Campinas, 13083-970, Campinas, SP, Brazil
[3]Kavli Institute at Cornell for Nanoscale Science, Ithaca, New York 14853, USA

(Received 30 May 2014; accepted 14 July 2014; published online 6 August 2014)

Optomechanical resonators suffer from the dissipation of mechanical energy through the necessary anchors enabling the suspension of the structure. Here, we show that such structural loss in an optomechanical oscillator can be almost completely eliminated through the destructive interference of elastic waves using dual-disk structures. We also present both analytical and numerical models that predict the observed interference of elastic waves. Our experimental data reveal unstressed silicon nitride (Si_3N_4) devices with mechanical Q-factors up to 10^4 at mechanical frequencies of $f = 102$ MHz ($fQ = 10^{12}$) at room temperature. *© 2014 AIP Publishing LLC*.
[http://dx.doi.org/10.1063/1.4892417]

Optomechanical resonators have fostered record detection of ultra-weak forces,[1] preparation of micromechanical oscillators close to their motional quantum ground states,[2,3] enabling self-sustaining mechanical oscillator dynamics,[4–6] and optomechanical photo-detection.[7] But like all micromechanical resonators, their performance suffers from the dissipation of mechanical energy. The dissipation of mechanical energy in such devices reduces their sensitivity, shortens their coherence time, increases their power consumption, and degrades the phase noise performance.[8,9] This mechanical dissipation is often dominated by anchor losses at the necessary supporting clamps,[10–12] among other mechanisms responsible for the overall dissipation such as thermo-elastic damping,[13] phonon scattering,[11] and defect relaxations.[14] Recent efforts in reducing anchor losses in micromechanical devices include using spoke design,[12,15] phononic bandgaps,[16,17] and materials with high internal stress.[18] The spoke design creates an artificial bottleneck of energy flow at the cost of structural rigidity, whereas phononic bandgap materials are less suitable for lower frequency resonators as the size of the unit cell scales up and they occupy larger real estate.

Here, we show that the structural loss of an optomechanical oscillator can be effectively eliminated through the destructive interference of elastic waves, by emulating the principle of a tuning fork resonator. A tuning fork resonator produces a long lasting sound when excited, as a result of its high mechanical quality factor. When a tuning fork vibrates, its two prongs oscillate 180° out of phase. The elastic wave produced from each prong largely cancels out leading to no net motion, therefore, no loss at the base. Here, in order to create the tuning fork effect, we use double-disk optomechanical resonators.[19,20]

We emulate the tuning fork principle using a dual-disk resonator, consisting of a pair of thin silicon nitride (Si_3N_4) disks separated by a narrow gap (Figs. 1(a) and 1(b)). The thin SiO_2 sacrificial layer mechanically couples the top and bottom resonators, allowing the mechanical waves to interfere. This sub-wavelength gap also results in the evanescent coupling of the optical fields, creating coupled optical modes that span both the top and the bottom disks. The attractive optical forces efficiently excite the antisymmetric (AS) mechanical modes, illustrated in Figs. 1(c) and 1(d) as the freestanding edges move in opposite directions. The symmetric (S) mechanical mode is, however, much less sensitive to the optical excitation.

When the two freestanding edges are identical, the structural dissipation of the antisymmetric mechanical mode is minimized. The origin of the anchor loss in our structures is due to the displacement induced in the clamping area by the oscillation of each freestanding edge. Such displacement radiates elastic waves towards the pedestal and the substrate and therefore dissipates energy from the mechanical resonance (Figs. 1(c) and 1(d)). The antisymmetric mechanical mode excited experiences much less structural loss than the symmetric mechanical mode due to the destructive interference between the elastic wave radiated from the top and the bottom disks.

In order to gain a physical intuition of the dissipation process, the dual-disk mechanical mode structure could be dissembled into simpler building blocks, the two freestanding edges (resonators T and B) emulating a tuning fork and the pedestal (resonator P), as depicted in Fig. 1(e). Since all the mechanical energy inside the pedestal leaks to the bulk substrate, the structural loss rate of the resonator can therefore be established as the mechanical coupling rate between the freestanding resonators and the pedestal resonators. The higher the coupling between the freestanding edges and the pedestal resonator, the more energy dissipation there is through the pedestal.

The coupling strength of the freestanding edges to the pedestal is reflected in their dispersion curves as a function of the middle SiO_2 layer thickness (t_m). In the case where there is no coupling, the mechanical frequencies of the edge modes would be independent of t_m, which is a parameter of

a)Author to whom correspondence should be addressed. Electronic mail: ml292@cornell.edu

 © 2014 AIP Publishing LLC

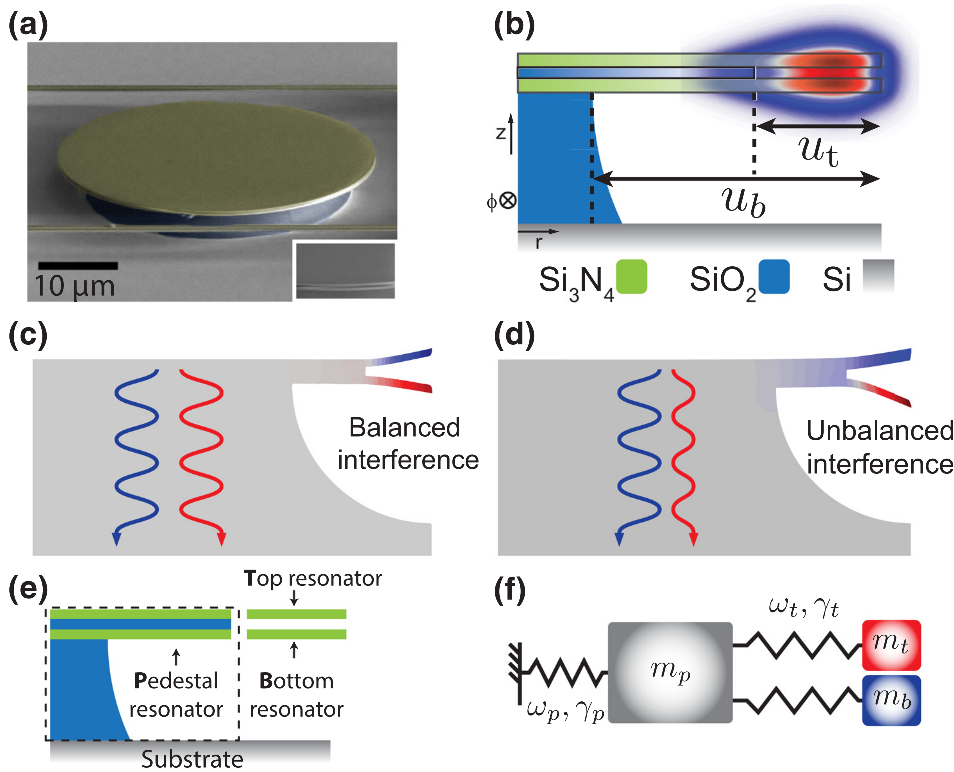

FIG. 1. Device schematic. (a) Scanning electron micrograph of the fabricated device. The inset is a close-up of the freestanding double-disk edges. The two horizontal strings are for supporting tapered fibers. (b) Schematic of the cross section of the device, u_t and u_b are the undercut depth of the top and bottom layers, respectively. The false-color scale shows the transverse electric optical mode profile which spans the top and the bottom disks. (c) and (d) Finite-element model showing the impact of the thickness difference of the top and bottom cantilever, leading to an unbalanced interference of the elastic wave emitted by the moving edges. (e) and (f) A lumped theoretical model consists of three masses: m_t and m_b for the two edges and m_p for the pedestal, each with mechanical frequencies ω_t, ω_b, ω_p and damping rate γ_t, γ_b, γ_p.

the pedestal mode. Therefore, the more sensitive the mode frequencies are to the SiO_2 layer thickness t_m, the stronger the coupling is to the pedestal. We numerically investigate the coupling strength between the freestanding edge and the pedestal resonators using a finite-element (FEM) solver (COMSOL) through varying the thickness t_m of the middle SiO_2 layer. As shown in Fig. 2(a), the antisymmetric (blue curve) mechanical mode stiffens and the symmetric (red curve) edge mode softens as t_m reduces. The rapid softening of the symmetric mechanical mode indicates a strong mechanical coupling to the pedestal mode. Whereas the antisymmetric mode displays an almost flat dispersion relation to t_m, indicating that the antisymmetric mode is insensitive to t_m of the pedestal resonator and therefore is weakly coupled to the pedestal mode. This is due to the canceling of the elastic wave from the two counter oscillating edges.

The vital role of the thickness difference in the freestanding edges can be visualized through the mechanical dissipation rate shown in Fig. 2(b). Our numerical simulation of the structural loss rate as a function of the thickness difference between the two edges in Fig. 2(b) confirms that indeed the loss rate is a minimum when the two disks are of equal

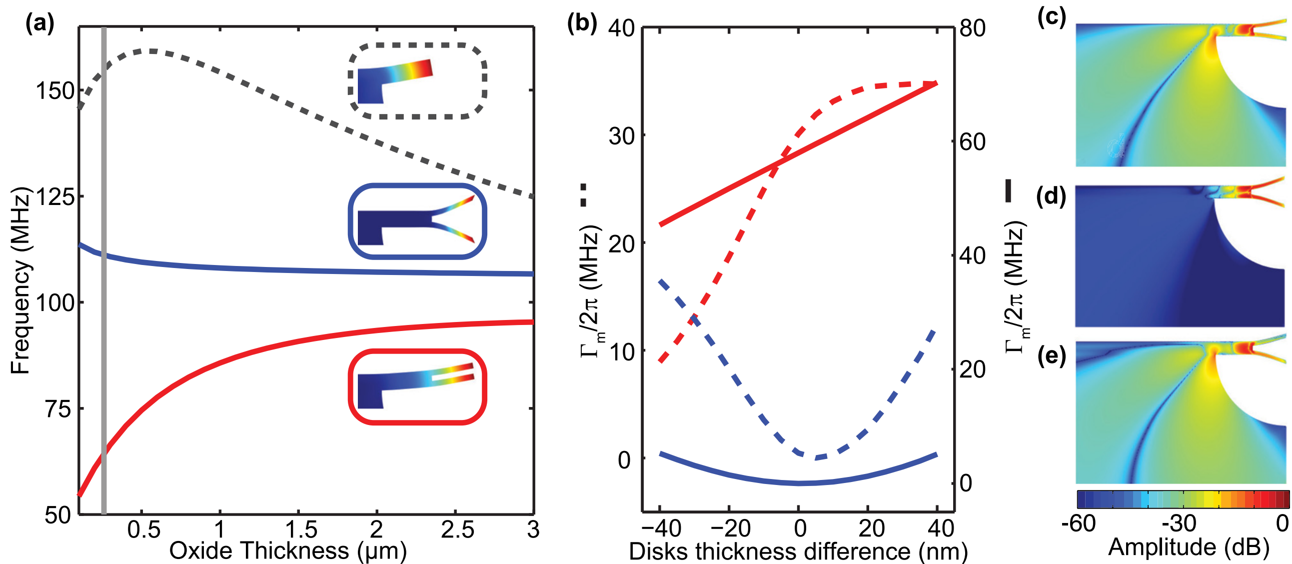

FIG. 2. Device simulations. (a) Dispersion of mechanical frequencies as function of middle SiO_2 thickness; grey-dashed: pedestal mode, solid-blue: AS mode, solid-red: S mode, vertical solid-grey shows position of 200 nm SiO_2 thickness. (b) Damping rate as function of top and bottom disks thicknesses difference for 3 μm (dashed, left scale) and 200 nm (solid, right scale) middle SiO_2 thickness, for the AS (blue) and S (red) modes. (c)-(e) $\hat{z}$ component of mechanical Poynting vector spatial distribution (false-color scale) for a top disk thicker $\delta t = 20$ nm (c), equal $\delta t = 0$ (e), and thinner $\delta t = -20$ nm (f) than the bottom one.

thickness. Note that for a thick sacrificial layer (dashed curves) the minimum structural loss for the antisymmetric edge mode occurs when the top disk is slightly thicker. This is due to the symmetry breaking from the finite undercut radius of the bottom disk. Figs. 2(c)–2(e) show the z-component of the mechanical energy flow (mechanical Poynting vector) for three top disk thickness differences when $t_m = 200$ nm. It is clear that the elastic wave radiation into the pedestal is drastically reduced when the two disks are of equal thickness.

We develop a pre-compensation technique to fabricate the freestanding edges of the double-disk structure and ensure that they are equal in thickness. We deposited a 240/200/220 nm Si_3N_4 /SiO_2/Si_3N_4 film stack on a silicon wafer with 3 μm of thermal SiO_2. The stoichiometric Si_3N_4 films are deposited via low pressure chemical vapor deposition technique and the SiO_2 layer is deposited via plasma-enhanced chemical vapor deposition and subsequently N_2 annealed at 1100 °C over 1 h. The 20 nm difference in the thickness of the two Si_3N_4 layers is designed to pre-compensate the change in their relative thickness as a result of the releasing wet etching step. We pattern the wafer with e-beam lithography and transfer the pattern with reactive ion etching (CHF_3/O_2). The devices are then undercut in a buffered oxide etch (6:1). This wet etching process has a finite selectivity to Si_3N_4 and SiO_2, roughly 1:100. Therefore, it not only etches SiO_2 at 80 nm/min but also removes Si_3N_4 at a slower rate of 0.8 nm/min. As the top Si_3N_4 layer is more exposed, it etches slightly faster than the bottom Si_3N_4 layer. After the designed release time, the resulting structure has two suspended Si_3N_4 layers with nearly identical thickness.

We experimentally demonstrate a high mechanical quality factor of 10^4 at 102.3 MHz, close to the material limited loss of Si_3N_4 at this frequency range.[18] This is more than a threefold improvement over previously demonstrated devices with uncompensated films whose typical measured mechanical quality factors are $Q_m = 2500$.[6] We measure the mechanical quality factor of our devices by coupling a low power continuous wave laser to the devices through a tapered optical fiber, as show in the schematic of Fig. 3(a). The devices are characterized inside a vacuum chamber (5–10 mTorr) at room temperature to minimize air damping. The mechanical spectrum can be observed through the optical transmission detected by a fast photodiode (Newport 1811A) which is connected to a radio-frequency (RF) spectrum analyzer. We test the optomechanical resonator by tuning the laser to an over-coupled optical resonance near 1530 nm with a loaded optical quality factor of 1.5×10^5. When the low power laser is slightly detuned from the cavity resonance, the thermal Brownian motion of the mechanical resonator is transduced to the optical signal as amplitude modulated RF signals. A typical RF spectrum of the detected photocurrent, which is proportional to thermal Brownian mechanical spectrum power density, is shown in Fig. 3(c) for an optimized cavity. The quality factor Q_m is obtained from a Lorenztian fit through the relation $Q_m = \omega_m/\delta\omega_m$, where $\delta\omega_m = 2\gamma_m$ is the full width half maximum of the thermal Brownian peak and ω_m and γ_m are the mechanical frequency

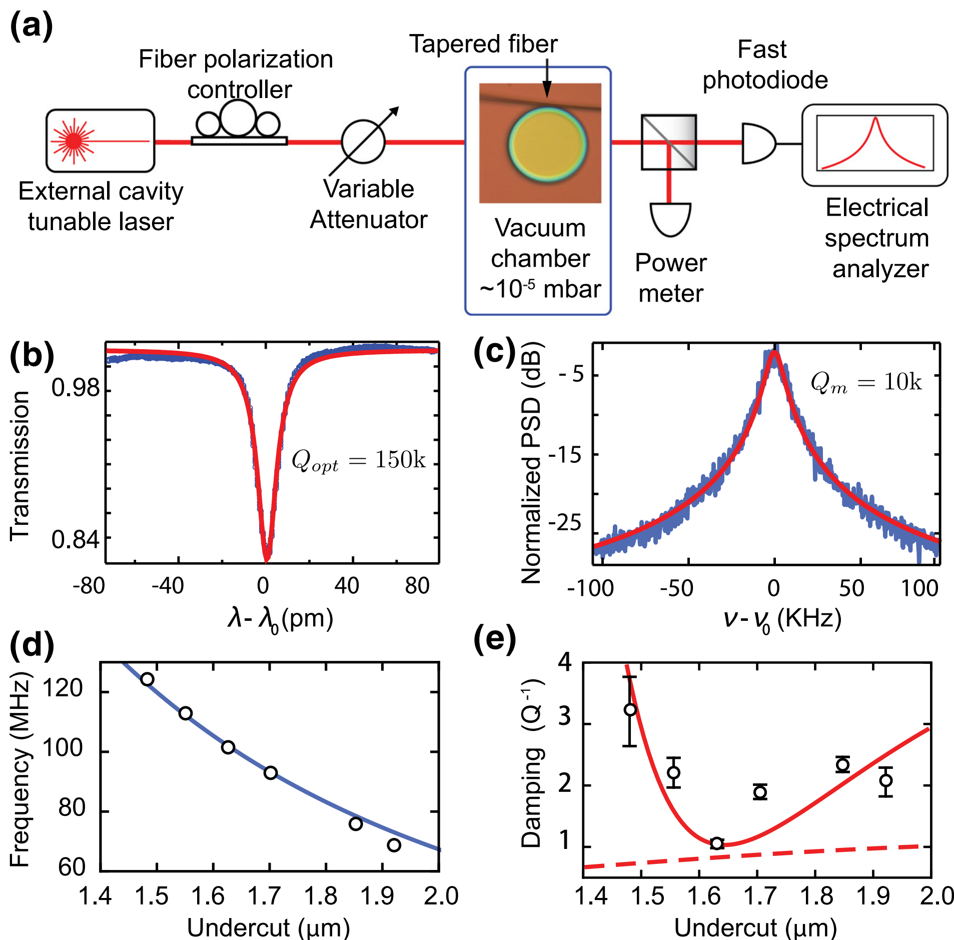

FIG. 3. Experimental results. (a) Simplified schematic of the experimental setup. (b) Optical transmission showing a resonance centered at $\lambda_0 = 1530.6$ nm with a loaded optical quality factor $Q_{opt} = 1.5 \times 10^5$. (c) Radio-frequency power spectral density of the transmitted optical signal. A typical AS mechanical mode resonant frequency centered at $\nu_0 = 102.3$ MHz for the optimized thickness device showing a quality factor $Q_m = 10^4$. (d) and (e) Measured mechanical frequency (d) and dissipation (e) of the devices etched through different times. The solid curves are the fitted analytical model prediction and the dashed line is the thermoelastic damping contribution. The error bars in (e) are obtained from the standard deviation among five identical devices.

and damping rate. We used an input optical power of 6 μW, well below the estimated threshold power of regenerative oscillation of 180 μW. At this input power level, the optomechanical feedback[21] does not affect the measured Q_m significantly. This is ensured by optimally detuning the laser on both sides of the optical resonance and verify that the difference between the blue and red-detuned Q-measurement is less than 1%. The measured mechanical frequencies (dissipation)) are shown as circles in Fig. 3(d) (Fig. 3(e)). The mechanical quality factors of the devices with pre-compensated layers have an average mechanical quality factor of $(8.0 \pm 0.8) \times 10^3$.

We show that the results from the numerical simulations and the experiment can be explained by a simple analytical lumped model of coupled resonators. We decompose the structure into the two freestanding edge resonators and the pedestal resonators as our qualitative analysis described previously. This analytical model agrees with the frequency dependence and the mechanical quality factors observed in both our numerical simulations and experimental results (Figs. 3(d) and 3(e)). In the analysis, we associate a mass-spring lumped model with each resonator identified in Fig. 1(e). The resulting coupled system is illustrated in Fig. 1(f). Note that when the masses move in opposite phase, there is no net motion of the pedestal and therefore the damping contribution from the pedestal damping γ_p is negligible. The normal modes of the coupled system are given by the eigenvectors of the matrix of the system

$$M(\Omega) = \begin{pmatrix} i\Delta_p + \gamma_p & i\kappa/2 & i\kappa/2 \\ i\kappa/2 & i\Delta_t + \gamma_t & i\beta/2 \\ i\kappa/2 & i\beta/2 & i\Delta_b + \gamma_b \end{pmatrix}, \quad (1)$$

where $\Delta_{p,t,b} \equiv \Omega - \omega_{p,t,b}$ is the detuning of the sought eigenvalue (Ω) and the lumped resonators frequencies ($\omega_{p,t,b}$), κ is the coupling rate between the top and bottom resonators to the pedestal, and ω_p the pedestal frequency. β is the coupling between the top and bottom resonators and $\gamma_{t,b,p}$ are the damping rate of the three oscillators. We assume the frequency dependence of the freestanding edges (ω_t,b) on the undercut (u_t) and thickness (t_i) is given by a circular-plate analytical model, $\omega_i(t_i) = x t_i u_t^{-2} E^{1/2}[12\rho(1-\nu^2)]^{-1/2}$, where $(E, \rho, \nu) = (250\,\mathrm{GPa}, 3100\,\mathrm{kg/m^3}, 0.25)$ are, respectively, the Young modulus, density, and the Poisson ratio for Si_3N_4. The numerical factor $x \sim 1.4$ is comparable to the value obtained by solving the plate problem with a clamped-free boundary condition.[22] By solving the characteristic equation given by $\det[M(\Omega)] = 0$, we obtain a complex eigenvalue (Ω) whose real and imaginary parts correspond to the mechanical frequency and damping of the normal modes, respectively. The solid blue and red lines in Figs. 3(d) and 3(e) show the fitted model prediction for the mechanical frequency and dissipation ($Q^{-1} = 2\mathrm{Im}[\Omega]/\mathrm{Re}[\Omega]$), respectively. The bare frequencies $\omega_{p,t,b}$ (u_t) are calculated from the analytical circular-plate analytical model and is also used to calculated the bare damping rates ($\gamma_t, b = \omega_{p,t,b}/(2Q_{t,b})$), with the bare quality factors ($Q_{t,b}$) inferred from FEM simulations. Since the model parameters impact very distinctively the real and imaginary parts of the complex eigenvalue, they were iteratively adjusted using both the measured frequencies (Fig. 3(d)) and damping rates (Fig. 3(e)). The fitted parameters are given by (Q_p, κ,β,x) = (1.2; 110 MHz, 5.96 MHz, 1.36) for which their initial values are estimated also by FEM simulations. When the structural loss is eliminated, the dominant loss will be thermoelastic damping. We show in Fig. 3(e), dashed-red line, the fundamentally limited dissipation based on thermoelastic damping prediction using the typical Si_3N_4 parameters $(c_p, \kappa_t, \alpha, T) = (710\,\mathrm{JK^{-1}}; 3.2\,\mathrm{Wm^{-1}K^{-1}}; 2\times10^{-6}\,\mathrm{K^{-1}}, 300\,\mathrm{K})$, representing, respectively, the specific heat, thermal conductivity, thermal expansion coefficient, and temperature.[13,18,23,24] This shows that our demonstrated device is within a factor of 1.3 of the material limited damping. Despite the simplicity of the model, the obtained fit parameters are in good agreement with values inferred from the FEM simulations.

Reducing the structural loss using destructive elastic wave interference is not only limited to double disk optomechanical oscillators. Using the same methodology, one could design, for example, an identical pair of loosely spaced singly or doubly clamped cantilevers. When they are excited in an anti-symmetric fashion, their support loss can be eliminated. Our method opens a path towards the deterministic design of micro- and nanomechanical resonators that are limited only by material losses.

We acknowledge Professor Paulo Nussenzveig for helpful discussions. This work was performed in part at the Cornell Nano-Scale Science and Technology Facility (a member of the National Nanofabrication Users Network), which was supported by NSF, its users, Cornell University, and Industrial users. The authors gratefully acknowledge support from DARPA for Award No. W911NF11 10202, supervised by Dr. Jamil AboShaeer. G.S.W. acknowledges FAPESP and CNPq INCT Fotonicom for financial support in Brazil.

[1]E. Gavartin, P. Verlot, and T. J. Kippenberg, Nat. Nanotechnol. **7**, 509 (2012).
[2]J. Chan, T. P. Mayer Alegre, A. H. Safavi-Naeini, J. T. Hill, A. Krause, S. Groeblacher, M. Aspelmeyer, and O. J. Painter, Nature **478**, 89 (2011).
[3]E. Verhagen, S. Deleglise, S. Weis, A. Schliesser, and T. J. Kippenberg, Nature **482**, 63 (2012).
[4]F. Marquardt, J. Harris, and S. Girvin, Phys. Rev. Lett. **96**, 103901 (2006).
[5]M. Poot, K. Y. Fong, M. Bagheri, W. Pernice, and H. X. Tang, Phys. Rev. A **86**, 053826 (2012).
[6]M. Zhang, G. Wiederhecker, S. Manipatruni, A. Barnard, P. McEuen, and M. Lipson, Phys. Rev. Lett. **109**, 233906 (2012).
[7]S. Tallur and S. A. Bhave, Nano Lett. **13**, 2760 (2013).
[8]K. L. Ekinci and M. L. Roukes, Rev. Sci. Instrum. **76**, 061101 (2005).
[9]K. J. Vahala, Phys. Rev. A **78**, 023832 (2008).
[10]D. M. Photiadis and J. A. Judge, Appl. Phys. Lett. **85**, 482 (2004).
[11]R. Lifshitz, Physica B: Condens. Matter **316–317**, 397 (2002).
[12]G. D. Cole, I. Wilson-Rae, K. Werbach, M. R. Vanner, and M. Aspelmeyer, Nat. Commun. **2**, 231 (2011).
[13]R. Lifshitz and M. Roukes, Phys. Rev. B **61**, 5600 (2000).
[14]O. Arcizet, R. Rivière, A. Schliesser, G. Anetsberger, and T. J. Kippenberg, Phys. Rev. A **80**, 021803 (2009).
[15]G. Anetsberger, R. Rivière, A. Schliesser, O. Arcizet, and T. J. Kippenberg, Nat. Photonics **2**, 627 (2008).
[16]F.-C. Hsu, J.-C. Hsu, T.-C. Huang, C.-H. Wang, and P. Chang, J. Phys. D: Appl. Phys. **44**, 375101 (2011).
[17]M. Eichenfield, J. Chan, R. M. Camacho, K. J. Vahala, and O. J. Painter, Nature **462**, 78 (2009).
[18]S. S. Verbridge, J. M. Parpia, R. B. Reichenbach, L. M. Bellan, and H. G. Craighead, J. Appl. Phys. **99**, 124304 (2006).

[19]G. S. Wiederhecker, L. Chen, A. Gondarenko, and M. Lipson, Nature **462**, 633 (2009).
[20]J. Rosenberg, Q. Lin, and O. J. Painter, Nat. Photonics **3**, 478 (2009).
[21]T. J. Kippenberg and K. J. Vahala, Science **321**, 1172 (2008).
[22]Y. Sun and H. Tohmyoh, J. Sound Vib. **319**, 392 (2009).
[23]Y. Sun and M. Saka, J. Sound Vib. **329**, 328 (2010).
[24]K. Y. Yasumura, T. D. Stowe, E. M. Chow, T. Pfafman, T. W. Kenny, B. C. Stipe, and D. Rugar, J. Microelectromech. Syst. **9**, 117 (2000).